RESEARCH ARTICLE

Figures and figure supplements

Intrinsic mechanisms in the gating of resurgent Na^+ currents

Joseph L Ransdell *et al*

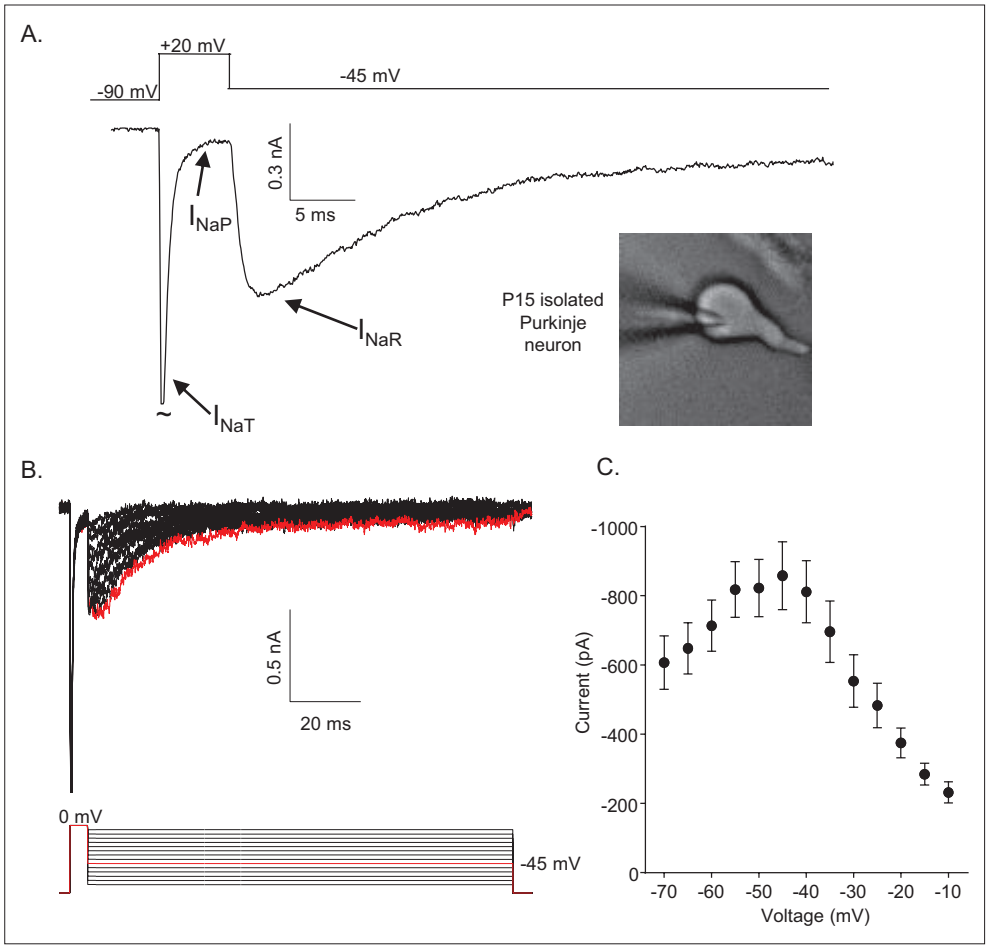

Figure 1. Mouse cerebellar Purkinje neurons express three voltage-gated sodium (Nav) current components. (**A**) Representative recording of the transient (I_{NaT}), persistent (I_{NaP}), and resurgent (I_{NaR}) components of the Nav currents in an isolated neonatal mouse cerebellar Purkinje neuron. The voltage-clamp paradigm is displayed above the current record, and the labelled arrows indicate the three Nav current components. (**B**) I_{NaR} waveforms, recorded during hyperpolarizing voltage steps to various potentials ranging from –70 to –10 mV, following 5 ms depolarizing voltage steps to 0 mV from a holding potential (HP) of –80 mV; the voltage-clamp paradigm is shown below the current records. The current record highlighted in red was recorded during the –45 mV hyperpolarizing voltage step (also indicated in *red* in the illustrated voltage-clamp paradigm). (**C**) Mean ± SEM (n = 15) peak I_{NaR} amplitudes are plotted as a function of the hyperpolarizing test potential; the peak I_{NaR} is recorded at approximately –45 mV.

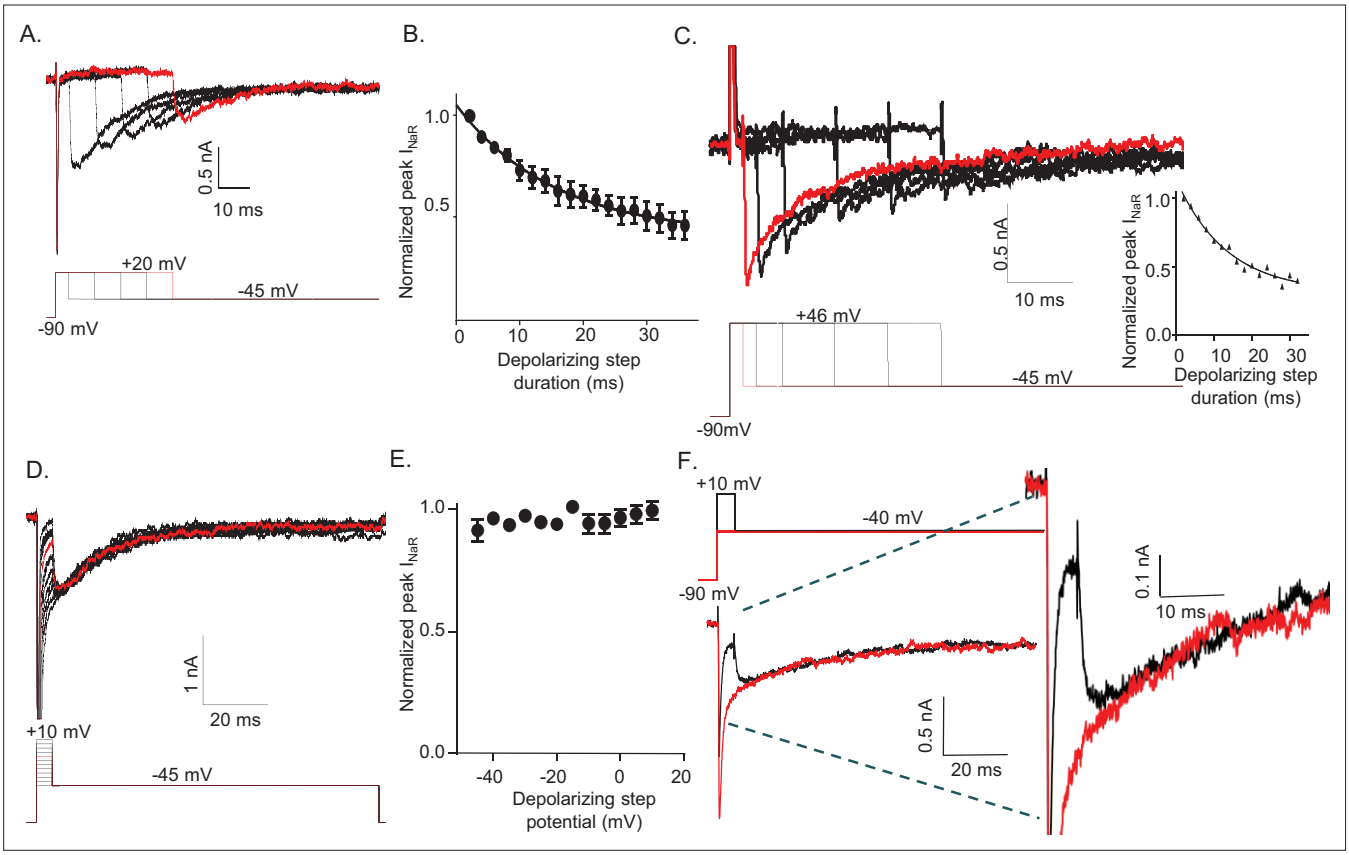

Figure 2. The amplitude of resurgent voltage-gated sodium current (I_{NaR}) is determined by the duration of the prior membrane depolarization. (**A**) In a neonatal mouse cerebellar Purkinje neuron, I_{NaR} was revealed on membrane hyperpolarizations following depolarizing voltage steps to +20 mV of varying durations; the voltage-clamp paradigm is shown below the current records. (**B**) Peak I_{NaR} amplitudes, evoked at –45 mV following each depolarizing voltage step to +20 mV, were measured and normalized to the maximal peak I_{NaR} (measured in the same cell). The mean ± SEM (n = 12) normalized peak I_{NaR} amplitudes are plotted as a function of the duration of the depolarizing voltage step. The attenuation of peak I_{NaR} as a function of the duration of the depolarizing voltage step was well described by a single exponential with a mean ± SEM time constant of 15.5 ± 0.5 ms (n = 12). (**C**) The dependence of I_{NaR} on the duration of the depolarizing voltage step was also measured with reduced (50 mM) extracellular and increased intracellular (15 mM) sodium, resulting in a Na^+ reversal potential of +30 mV. Under these conditions, depolarizing voltage steps to +46 mV evoked outward I_{NaT}. Peak I_{NaR} amplitudes, revealed during hyperpolarizing voltage steps to –45 mV, however, were also found to vary as a function of the duration of the depolarizing voltage step, revealing that I_{NaR} and the time-dependent attenuation of I_{NaR} are not affected by the direction (inward versus outward) of Na^+ flux during the depolarizing voltage step. The peak amplitudes of I_{NaR}, evoked at –45 mV following each depolarizing voltage step, were measured in each cell and normalized to the maximal I_{NaR} amplitude (in the same cell). As is evident from the representative records and the plot of normalized peak I_{NaR} amplitudes (on the right), the attenuation of I_{NaR} as a function of the duration of the depolarizing voltage steps to +46 mV is also well described by a single exponential with a mean ± SEM time constant of 13.8 ± 1.1 ms (n = 6), a value similar to that observed when I_{NaT} was inward (**B**). (**D**) Representative I_{NaR} waveforms, recorded directly on repolarizations to –45 mv following 5 ms depolarizations to various membrane potentials from a –90 mV HP, are shown; the voltage-clamp protocol is shown below the current records. (**E**) The mean ± SEM (n = 6) normalized peak I_{NaR} amplitudes are plotted as a function of potential of the depolarizing voltage step. (**F**) Representative voltage-clamp recordings of Nav currents evoked (in the same cell) on direct depolarization to –40 mV from an HP of –90 mV (*red*) and on hyperpolarization to –40 mV following a 5 ms depolarizing voltage step to +10 mV (*black*) from the same HP; the voltage-clamp protocols are shown above the current records and the currents are shown on an expanded scale on the right. In panels A, C, D, and F, the currents in red were recorded during the voltage-clamp paradigms (shown below or above) depicted in red.

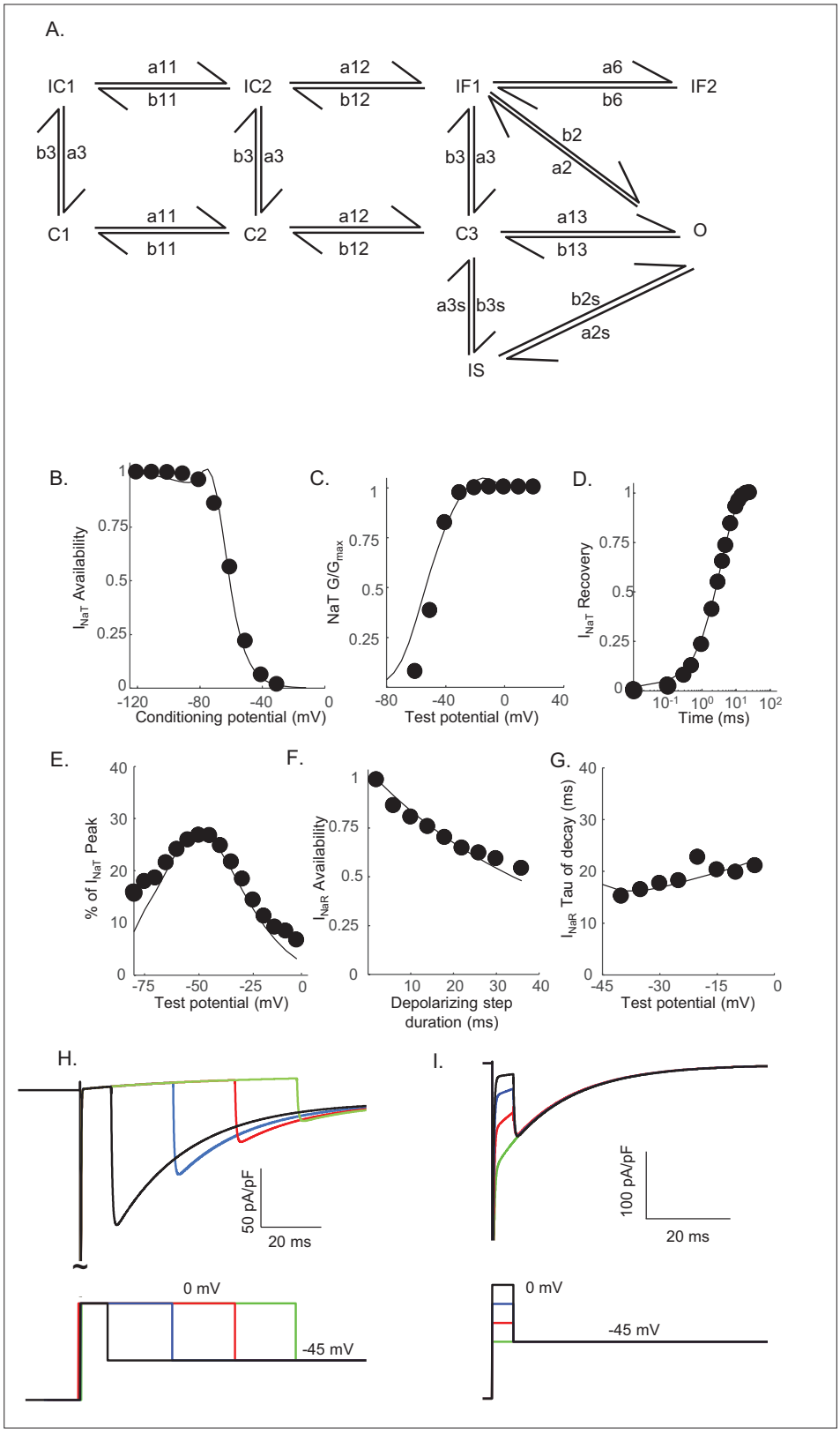

Figure 3. Novel Markov kinetic state model of voltage-gated sodium (Nav) channel gating in cerebellar Purkinje neurons. A novel Markov kinetic state model was developed with parallel fast inactivating (IF1, IF2) and slow inactivating (IS) gating pathways (**A**). The model was numerically optimized (see Materials and methods) by simulating the data generated using voltage-clamp protocols identical to those used in the experiments to

Figure 3 continued on next page

Figure 3 continued

determine the detailed time- and voltage-dependent properties of the Nav currents in cerebellar Purkinje neurons. The various rate constants in the model were numerically optimized to recapitulate the measured properties of I_{NaT}, I_{NaP}, and I_{NaR} including the voltage dependences of steady-state inactivation (**B**) and activation (**C**) of I_{NaT}, and the kinetics of I_{NaT} recovery from inactivation (**D**). The model also reproduces the measured properties of I_{NaR}, including the magnitude of I_{NaR} relative to I_{NaT} (**E**), the attenuation of the peak I_{NaR} amplitude as a function of the duration of the depolarizing voltage steps (**F**), and the kinetics of the decay (inactivation) of peak I_{NaR} amplitudes (**G**). Filled circles represent the mean experimental data and the lines represent the results of the simulation. The model successfully reproduces the observed, time-dependent attenuation of peak I_{NaR} amplitudes that is evident experimentally on membrane hyperpolarizations following depolarizing voltage steps of varying durations (**H**), and the finding that the peak amplitude of I_{NaR} is not affected by the potential of the depolarizing voltage step (**I**).

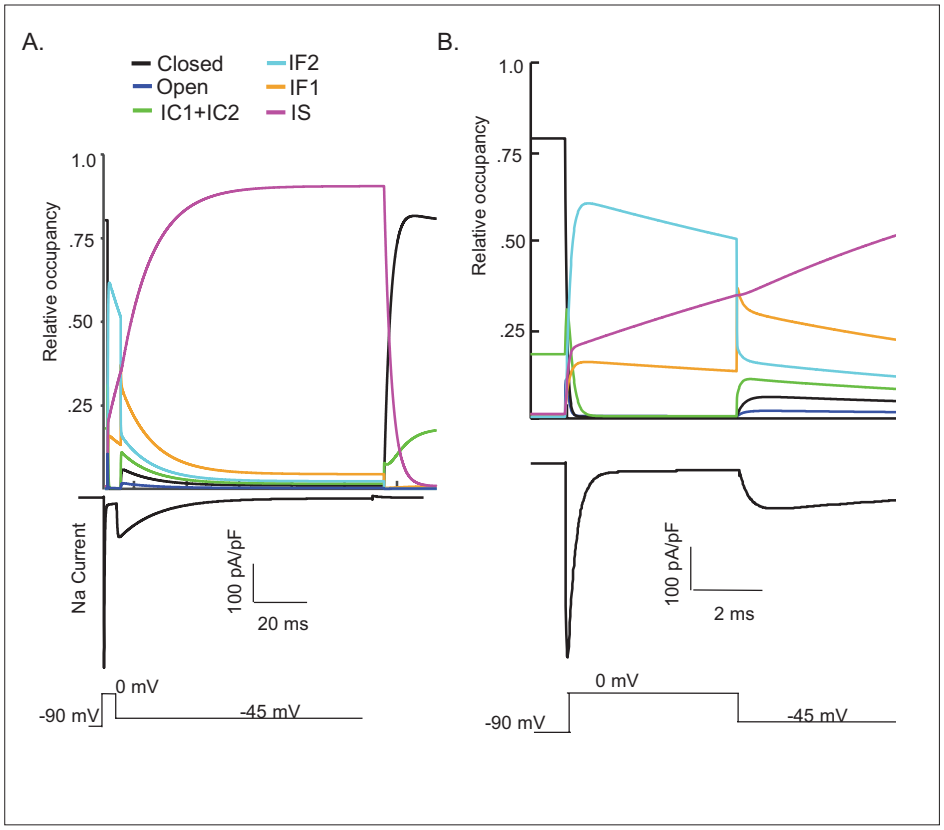

Figure 4. Kinetic state transitions during voltage-clamp simulations that evoke voltage-gated sodium current (I_{NaR}). There are two parallel pathways of voltage-gated sodium (Nav) channel inactivation (IF1/IF2 and IS) in the novel Markov kinetic state model developed here (***Figure 3***). The occupancies of these states and of the other (i.e., closed, open, etc.) channel gating states during a simulated voltage-clamp protocol, in which I_{NaR} is revealed on membrane hyperpolarization to –45 mV following a brief (5 ms) depolarizing voltage step to 0 mV from a holding potential of –90 mV, are plotted as a function of time in (**A**). The simulated voltage-clamp records and the experimental paradigm are illustrated below the gating state occupancy plot. Expanded (in time) views of the gating state occupancies and the simulated Nav currents are presented in (**B**). In the gating state occupancy plots, *black* represents the closed state, *blue* represents the open state, *green* represents the IC1+ IC2 states, *aqua* represents the IF2 state, *orange* represents the IF1 state, and *purple* represents the IS state.

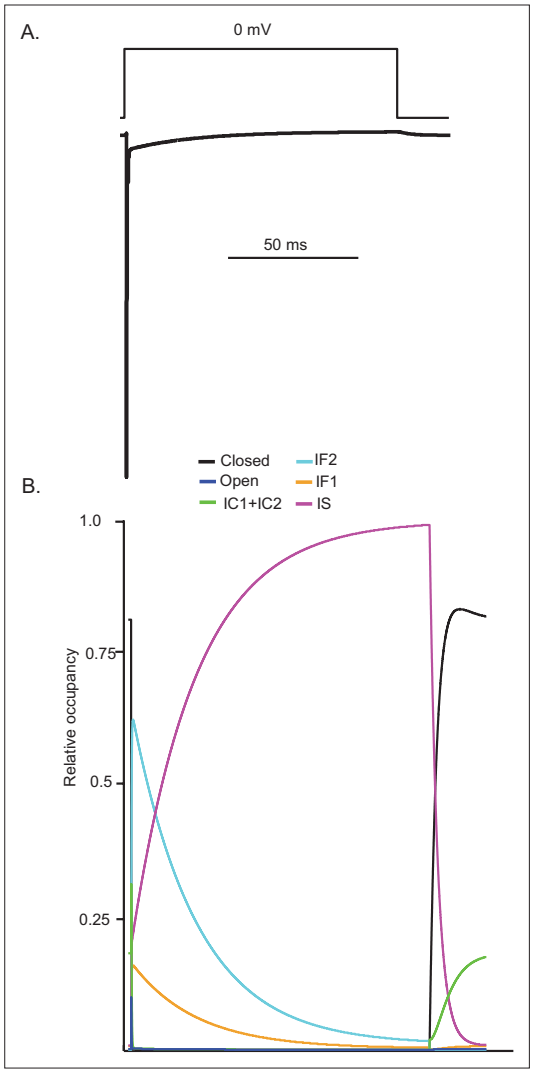

Figure 4—figure supplement 1. Simulations reveal that, similar to hyperpolarizing voltage steps, prolonged depolarization results in the accumulation of voltage-gated sodium (Nav) channels in the IS state. Using the novel Markov model developed here (***Figure 3A***), a prolonged depolarizing voltage step to 0 mV produces a rapidly activating Nav current with two kinetically distinct inactivating components (**A**). The gating state occupancy plot (**B**) reveals that Nav channels transition first into the IF2 state (*aqua*) and subsequently into the IS state (*orange*).

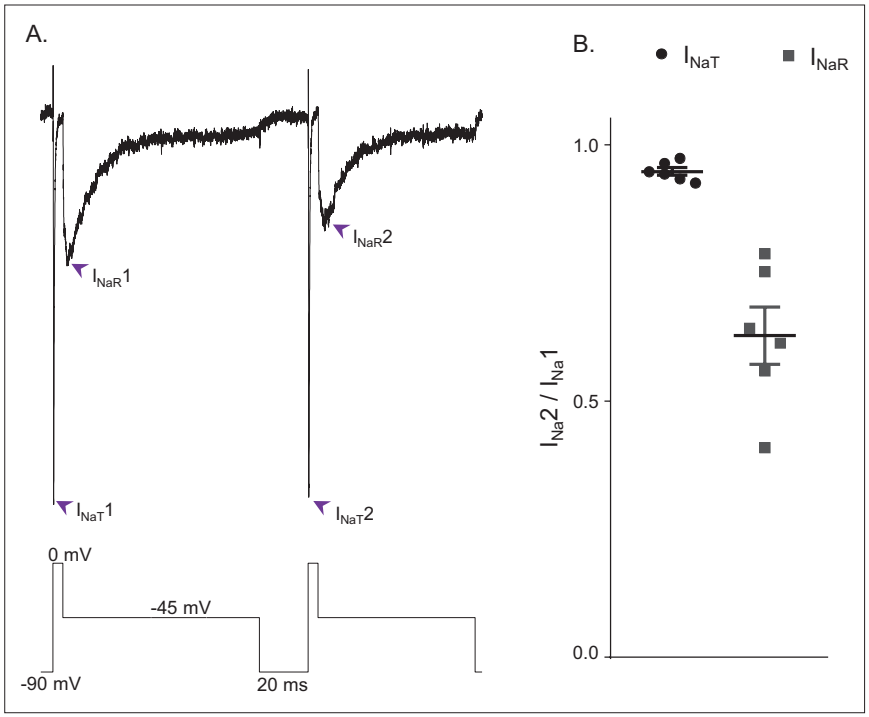

Figure 5. I_{NaR} and I_{NaT} display distinct rates of recovery from inactivation. (**A**) Representative voltage-gated sodium (Nav) currents recorded in a mouse cerebellar Purkinje neuron during a voltage-clamp paradigm designed to determine if the relative rates of recovery from inactivation of I_{NaT} and I_{NaR} are distinct. Inward Nav currents were recorded during sequential and identical voltage-clamp steps (to 0 mV for 5 ms and to –45 mV for 100 ms), separated by a brief (20 ms) hyperpolarizing step to –90 mV; the voltage-clamp paradigm is shown below the current records. As is evident, the amplitude of I_{NaR} (at –45 mV) during the second voltage-clamp step to –45 mV was attenuated more than I_{NaT} (during the second step to 0 mV). Similar results were obtained in five additional Purkinje neurons using the voltage-clamp paradigm shown. (**B**) Plot of the relative peak I_{NaT} (circles) and peak I_{NaR} (squares) amplitudes measured during the second voltage-clamp steps (to 0 and –45 mV), compared with the first. As is evident, the relative amplitude of I_{NaR} is reduced (0.63 ± .05; n = 6) to a greater extent (paired Student's t-test; p = .00039) than I_{NaT} (0.95 ± 0.01; n = 6). The mean ± SEM (n = 6) relative I_{NaT} and I_{NaR} amplitudes are also indicated.

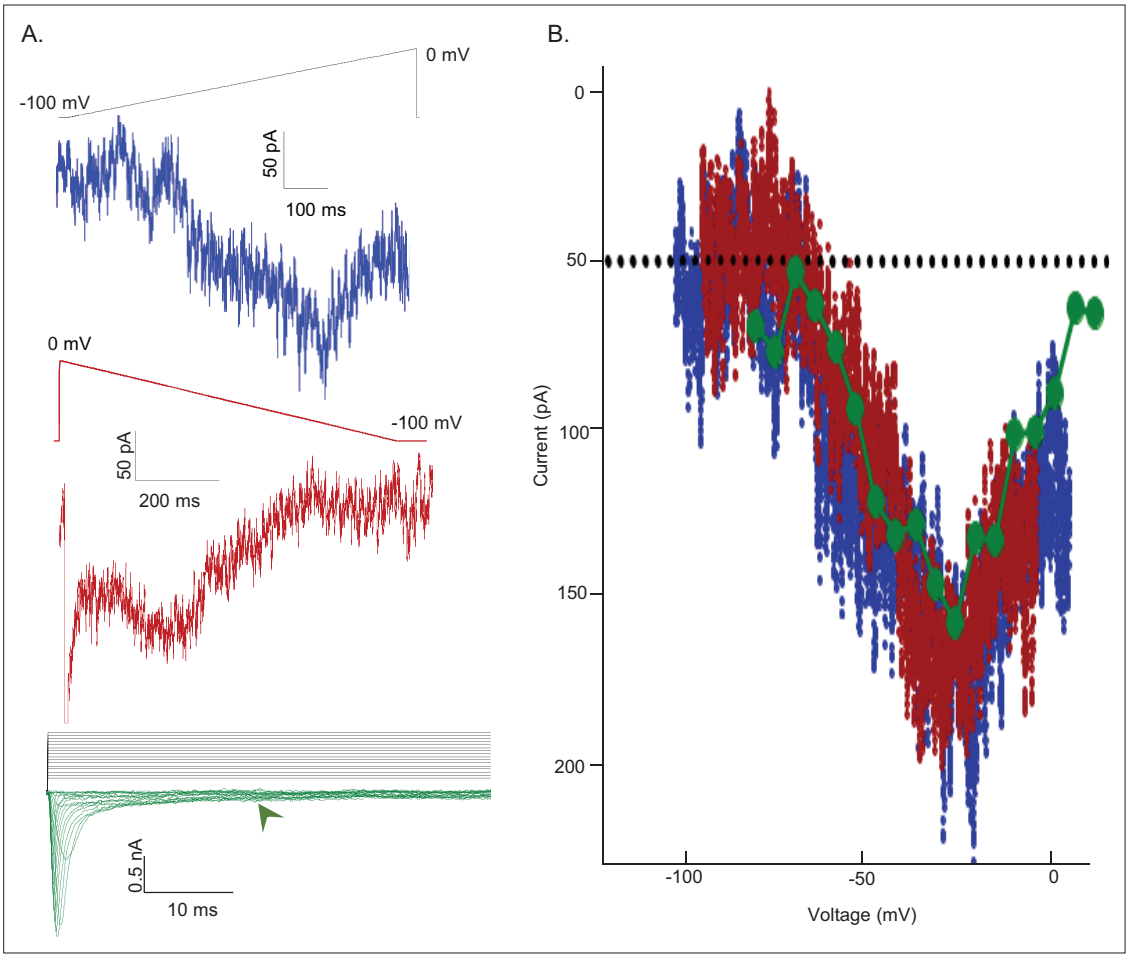

Figure 6. Voltage dependences of activation of I_{NaR} and I_{NaP} are indistinguishable. (**A**) To test the hypothesis that non-inactivating voltage-gated sodium (Nav) channels underlie I_{NaR}, a depolarizing voltage ramp (*blue*) protocol (from –100 to 0 mV at 0.12 mV/ms) and a steady-state voltage step (*green*) protocol (with depolarizations from a holding potential of –100 mV to test potentials ranging from –75 to 10 mV in 5 mV increments) were used to reveal the magnitude and voltage-dependent properties of the non-inactivating (persistent) component of the Nav current, I_{NaP}. In addition, a hyperpolarizing voltage ramp (from 0 to –100 mV at 0.12 mV/ms or dV/dt) was used to reveal both I_{NaR} and I_{NaP}. Note that as I_{NaR} decays (see ***Figure 2B***) during the hyperpolarizing voltage-ramp, the relative amplitudes of I_{NaR} and I_{NaP} vary during the ramp; the sum of the two current components, not the amplitudes of the individual components, therefore, are measured. The three representative records shown were obtained from the same Purkinje neuron. (**B**) The current-voltage relationships, derived from the records presented in (**A**) are plotted (in the corresponding color). From the records shown in the lowest panel of (**A**), the amplitudes of the steady-state inward currents at 25 ms at each test potential are plotted as points (green); the current amplitudes determined (at 2 ms intervals) from the ramp protocols (*red* and *blue* traces) are also plotted. As is evident, the current-voltage relations of the Nav currents recorded using the three different voltage-clamp protocols overlap; the magnitudes of the inward Nav currents are also indistinguishable. Similar results were obtained in four additional Purkinje neurons.

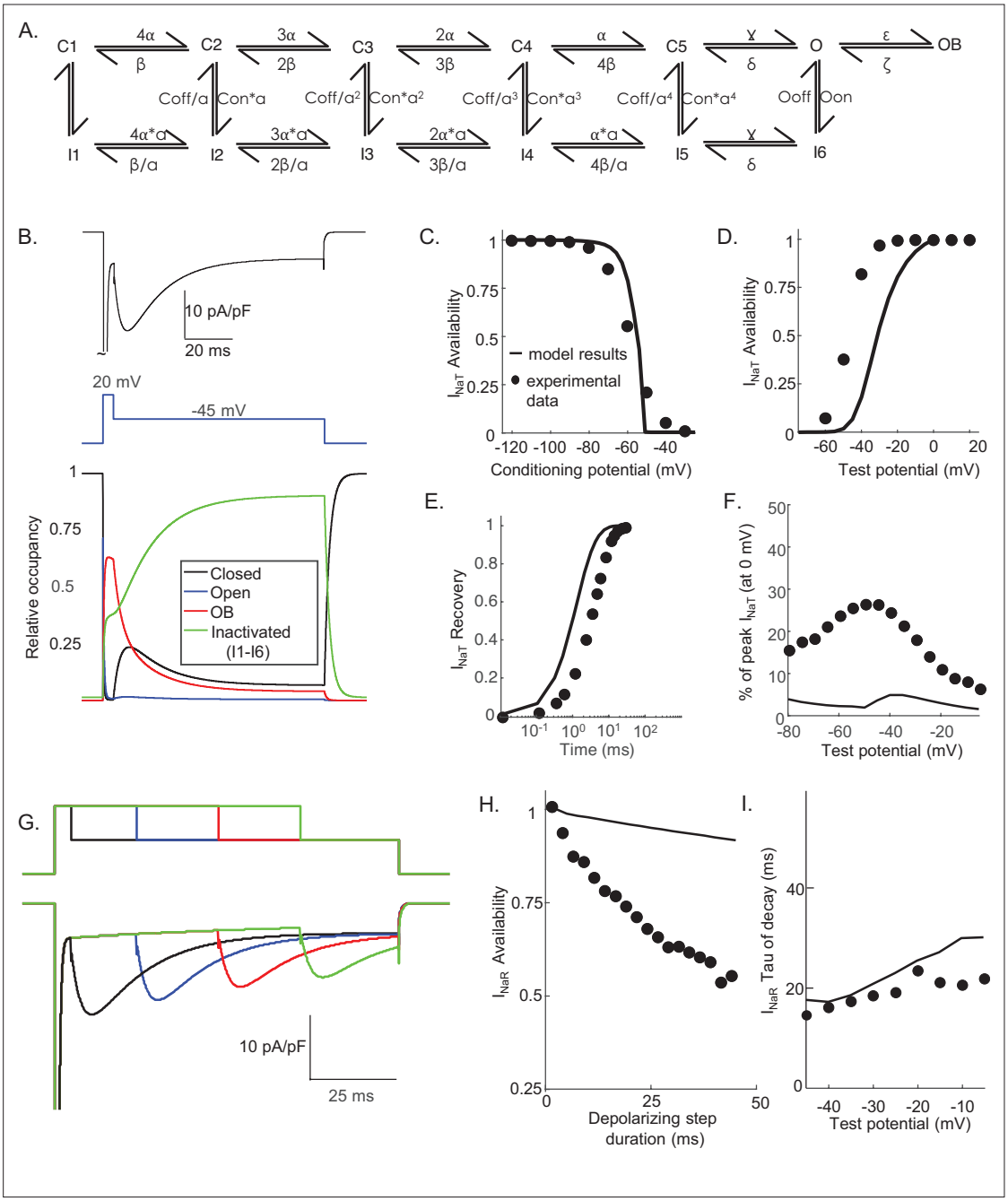

Figure 7. Simulations using the Raman-Bean model of voltage-gated sodium (Nav) channel gating do not recapitulate the acquired voltage-clamp data. (**A**) The previously described Markov kinetic state model of Nav channel gating in mouse cerebellar Purkinje neurons (***Raman and Bean, 2001***) is illustrated. (**B**) Representative simulated inward Nav current waveforms, produced by this (**A**) model using the voltage-clamp paradigm shown below the current records, are presented. The time-matched normalized occupancies of the combined closed (C1–C5, shown in *black*), open (O, shown in *blue*), open-blocked (OB, shown in *red*), and combined inactivated (I1–I6, shown in *green*) gating states are plotted below the voltage protocol. (**C–E**) Comparisons of the time- and voltage-dependent properties of I_{NaT} derived from simulations using the model in (**A**) with (our) experimental data obtained in recordings from mouse cerebellar Purkinje neurons (the same data as were used to generate the results in ***Figure 3***); filled circles represent the mean experimental data and the lines represent the results of the simulations. (**F**) Relative I_{NaR} amplitudes (normalized to peak I_{NaT} at 0 mV) are plotted as a function of the hyperpolarizing test potential. (**G**) Simulated I_{NaR} waveforms, produced on membrane hyperpolarizations to –45 mV following depolarizing voltage steps to +20 mV of varying durations, are shown. (**H**) Peak normalized I_{NaR} amplitudes (at –45 mV), derived from the simulations in (**G**), are plotted as a function of the duration of the prior +20 mV depolarizing voltage step (solid line), together with the mean experimental data (filled circles) obtained in recordings from mouse cerebellar Purkinje neurons (the same data as used to generate the results in ***Figure 3***). (**I**) The kinetics of I_{NaR} decay, derived from single exponential fits to the decay phases of the currents recorded at various membrane potentials, are presented in (**I**); the solid

Figure 7 continued on next page

Figure 7 continued

lines indicate the results of the simulations, and the filled circles are the mean experimental data obtained in recordings from mouse cerebellar Purkinje neurons (the same data as used to generate the results in ***Figure 3***).

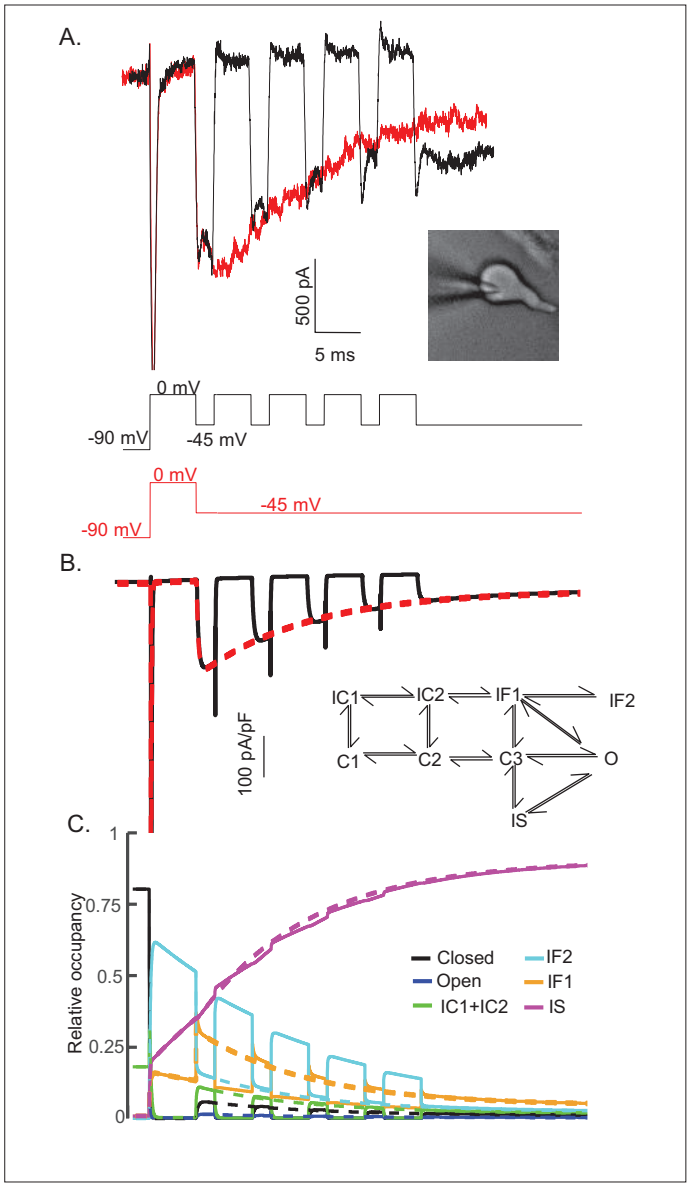

Figure 8. The time course and amplitude of I_{NaR} are recapitulated during repetitive brief depolarizing steps. To determine if two competing inactivation states underlie the observed differences in I_{NaT} and I_{NaR} recovery from inactivation (illustrated in ***Figure 5***), a protocol was developed to allow direct comparison of I_{NaR} recorded during a single (80 ms) hyperpolarizing voltage step to –45 mV (*red*), presented following a brief (5 ms) depolarization to 0 mV, with I_{NaR} recorded (in the same cell) at –45 mV during successive brief (2 ms) hyperpolarizing voltage steps interspersed with brief (5 ms) depolarizations to 0 mV (*black*). Representative records are shown in (**A**); the voltage-clamp paradigms are illustrated below the current records. Similar results were obtained in four additional Purkinje neurons. As is evident (**A**), the envelope of the currents generated using these two protocols superimpose, suggesting that the inactivation pathway responsible for I_{NaR} decay does not compete with fast inactivation. (**B**) Simulated current waveforms, generated using the same two voltage-clamp protocols illustrated in (**A**) with the novel kinetic state model presented in ***Figure 3A***, are shown. (**C**) Gating state occupancies for simulated current traces are shown with *black* representing the closed state, *blue* representing the open state, *green* representing the IC1+ IC2 states, *aqua* representing the IF2 state, *orange* representing the IF1 state, and *purple* representing the IS state. For direct comparison of the results of the simulations using the voltage-clamp protocols illustrated in (**A**) with the Raman-Bean gating model (2001), see ***Figure 8—figure supplement 1***.

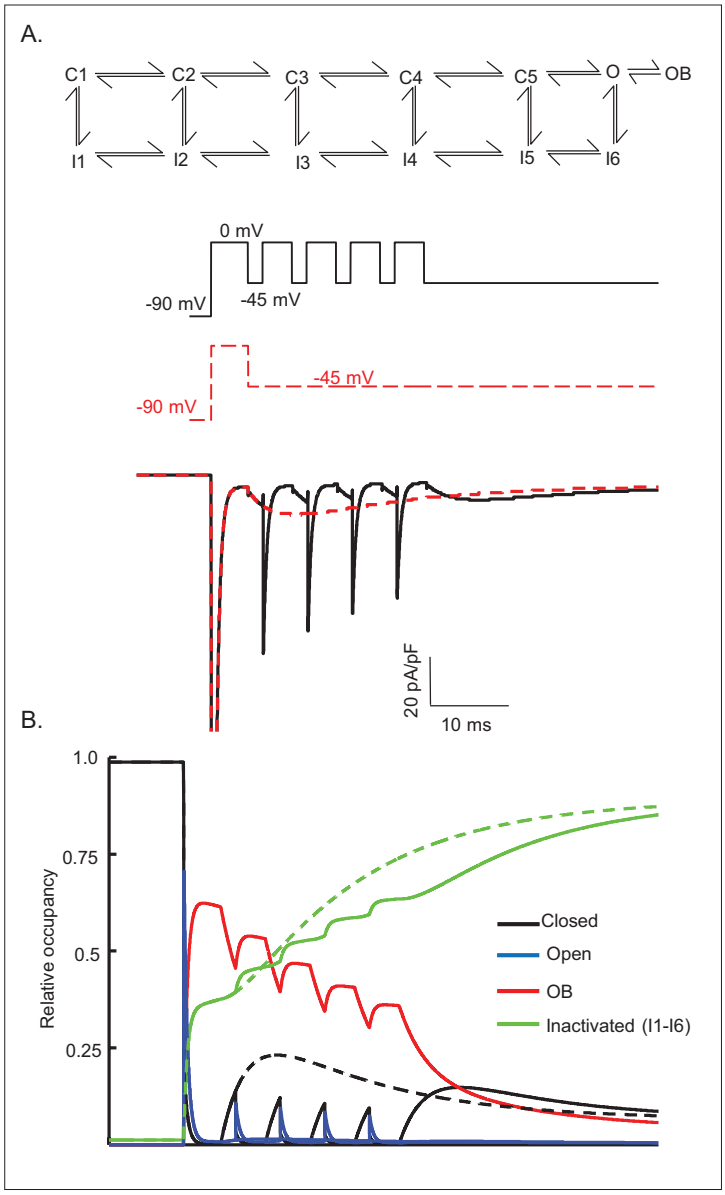

Figure 8—figure supplement 1. Gating state occupancies/transitions produced in the Raman-Bean model (with the voltage-clamp protocols used in ***Figure 8***). The Raman-Bean model (presented in ***Figure 7A***) does not reproduce the Nav currents recorded from a Purkinje neuron that is depolarized (to 0 mV) and repolarized (to –45 mV) repeatedly (see ***Figure 8A***); the voltage-clamp protocol and the simulated currents produced are shown in (**A**) as solid *black* lines. Nav current waveforms, simulated using the Raman-Bean model, in response to a sustained hyperpolarization to –45 mV following a brief (5 ms) depolarizing voltage step to 0 mV are also shown; the voltage-clamp protocol and the simulated currents are shown in (**A**) as dashed *red* lines. The gating state occupancy plot (**B**), presented on the same time scale as the voltage-clamp records, is shown; colors denote the various kinetic states with *black* representing the closed state, *blue* representing the open state, *red* representing the open-blocked (OB) state, and *green* representing the inactivated (**I1–I6**) states. The dashed lines are the gating state transitions associated with the dashed (*red*) current records in (**A**), and the solid lines are the gating state transitions associated with the solid (*black*) current records in (**A**).

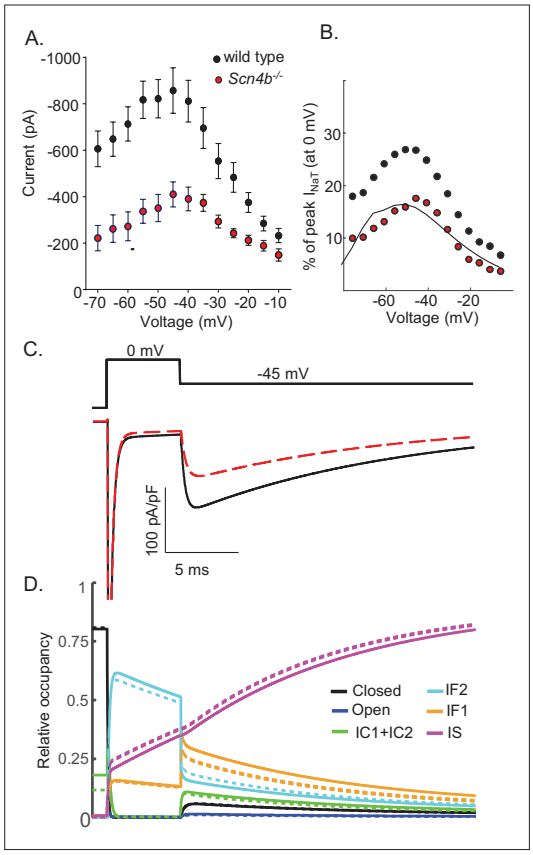

Figure 9. Promoting entry into the slow-inactivated state reduces voltage-gated sodium current (I_{NaR}) amplitudes. (**A**) Mean ± SEM peak I_{NaR} amplitudes, measured on membrane hyperpolarizations following brief depolarizing voltage steps to +10 mV, in wild type (*black*) and *Scn4b*$^{-/-}$ (*red*) mouse cerebellar Purkinje neurons are plotted as a function of membrane voltage are shown (data were reproduced with permission from ***Ransdell et al., 2017***). Peak I_{NaR} amplitudes in individual wild type and *Scn4b*$^{-/-}$ cells were also normalized to peak I_{NaT} measured (at 0 mV) in the same cell, and the mean I_{NaR} as a percentage of peak I_{NaT} in wild type (*black*) and *Scn4b*$^{-/-}$ (*red*) cells are plotted (as points) in (**B**); the solid line is the normalized relative I_{NaR}/I_{NaT} generated by the *Scn4b*$^{-/-}$ model. (**C**) Consistent with the experimental data, the kinetics of I_{NaR} are not affected measurably by the loss of *Scn4b* (Navβ4) in the model, whereas I_{NaR} amplitudes are reduced to ~50% of wild type I_{NaR} levels (**C**). A time-locked plot of the gating state transitions (**D**) indicates that I_{NaR} amplitudes are reduced in the *Scn4b*$^{-/-}$ model (dashed lines) due to a decrease in IF2 occupancy and an increase in IS occupancy. In this gating state occupancy plot, *black* represents the closed state, *blue* represents the open state, *green* represents the IC1+ IC2 states, *aqua* represents the IF2 state, *orange* represents the IF1 state, and *purple* represents the IS state.